Materials Today Bio 13 (2022) 100216

Contents lists available at ScienceDirect

Materials Today Bio

journal homepage: www.journals.elsevier.com/materials-today-bio

Fabrication of gelatin-based and Zn^{2+}-incorporated composite hydrogel for accelerated infected wound healing

Bailong Tao [a,b,1], Chuanchuan Lin [c,1], Xian Qin [d], Yonglin Yu [e], Ai Guo [f], Kai Li [f], Hongchuan Tian [g], Weiwei Yi [h], Dengliang Lei [i], Yue Chen [a], Lixue Chen [a,*]

[a] Laboratory Research Center, The First Affiliated Hospital of Chongqing Medical University, Chongqing, 400016, China
[b] Key Laboratory of Biorheological Science and Technology, Ministry of Education College of Bioengineering, Chongqing University, Chongqing, 400044, China
[c] Department of Blood Transfusion, Laboratory of Radiation Biology, The Second Affiliated Hospital, Third Military Medical University, Chongqing, 400037, China
[d] Department of Reproductive Endocrinology, Chongqing Health Center for Women and Children, Chongqing, 401147, China
[e] Department of Pathology, Affiliated Hospital of Zunyi Medical University, Zunyi, 563003, China
[f] Department of Orthopedics, The Third Affiliated Hospital of Chongqing Medical University, Chongqing, 400016, China
[g] Department of Orthopedics, The Second Affiliated Hospital of Chongqing Medical University, Chongqing, 400010, China
[h] Department of Rehabilitation Medicine, The First Affiliated Hospital of Chongqing Medical University, China
[i] Department of Hepatobiliary Surgery, The First Affiliated Hospital of Chongqing Medical University, Chongqing, China

ARTICLE INFO

Keywords:
Gelatin
Dopamine
Zinc ions
Antibacterial hydrogel
Infected wound healing

ABSTRACT

Gelatin-based hydrogels have a broad range of biomedical fields due to their biocompatibility, convenience for chemical modifications, and degradability. However, gelatin-based hydrogels present poor antibacterial ability that hinders their applications in treating infected wound healing. Herein, a series of multifunctional hydrogels (Gel@Zn) were fabricated through free-radical polymerization interaction based on gelatin methacrylate (GelMA) and dopamine methacrylate (DMA), and then immersed them into zinc nitrate solutions based on the metal coordination and ionic bonding interaction. These designed hydrogels wound dressings show strong antibacterial activity against *Escherichia coli* (*E. coli*) and *Staphylococcus aureus* (*S. aureus*) by increasing intracellular reactive oxygen species (ROS) level and changing bacterial membrane permeability. Meanwhile, the hydrogels exhibit good cytocompatibility, enhance the adhesion, proliferation, and migration of NIH-3T3 cells. Furthermore, Gel@Zn-0.08 (0.08 M Zn^{2+} immersed with Gel sample) presents a good balance between antibacterial effect, cell viability, and hemolytic property. Compared with 3 M commercial dressings, Gel@Zn-0.04, and Gel@Zn-0.16, the Gel@Zn-0.08 could significantly improve the healing process of *S. aureus*-infected full-thickness wounds *via* restrained the inflammatory responses, enhanced epidermis and granulation tissue information, and stimulated angiogenesis. Our study indicates that the Zn-incorporated hydrogels are promising bioactive materials as wound dressings for infected full-thickness wound healing and skin regeneration.

1. Introduction

Skin is the largest organ and also the first line of defense in the human body and is usually disturbed by external environments, such as perspiration, perceived temperature, pressure, and pathogenic bacterial infections [1,2]. *Staphylococcus aureus* (*S. aureus*) is a common disease-causing bacteria, which can lead to local purulent infection once the wound forms, thereby even life-threatening in severe cases [3,4]. Currently, to address this issue, numerous types of wound dressings, such as membranes, sponge, aerogel, scaffold, and hydrogels have been developed [5–7]. Among them, the hydrogel was widely used in accelerating wound healing, due to its three-dimensionally porous structure, high hydroscopicity and water holding property, good biodegradability and biocompatibility, and was similar to the natural extracellular matrix (ECM) [8,9]. However, the conventional hydrogel dressings lack inherent antibacterial properties, which is helpless for treating infected wounds [10]. To improve this situation, loading antibiotics to hydrogel has attributed extensive attention and has shown a certain positive effect on the treatment of infected wound healing [11,12]. Unfortunately, the emergence of drug-resistant bacteria further exacerbates their threat to

* Corresponding author.
E-mail address: chenlixue@hospital.cqmu.edu.cn (L. Chen).
[1] Bailong Tao and Chuanchuan Lin were co-first authors and contributed equally to this work.

https://doi.org/10.1016/j.mtbio.2022.100216
Received 2 December 2021; Received in revised form 27 January 2022; Accepted 7 February 2022
Available online 9 February 2022

human health due to the abuse of antibiotics [13]. Additionally, the photo-thermal antibacterial methods based on photothermal therapy could promote infected wound healing owing to local high temperature, nevertheless, it could inevitably lead to burns of normal tissues [6]. Consequently, it is urgent to design novel hydrogel dressings for infected wound healing with strong antibacterial ability based on antibiotic-free therapy and does not induce normal tissue damage.

Gelatin (Gel), a well-known natural protein, is the hydrolysis product of collagen derived from connective tissues in animal skin, bone, and tendon [14]. Importantly, Gel possesses abundant arginine-glycine-aspartic acid (RGD) sequences, which is beneficial for cell attachment and remodeling without grafting of RGD compared to other biomacromolecules-based hydrogels [15]. Besides, abundant attention has been paid to Gel-based hydrogel for biomedical applications because it has many available advantages such as being resourceful, biocompatible, degradable, and convenient for chemical modifications [16–19]. These characteristics implied that Gel-based hydrogel may be a promising candidate for trauma dressing. Our previous studies confirmed that Gel can be easily modified with methylacry chloride into gelatin methacrylate (GelMA), and the resulting gold-metal–organic frameworks-embedded sodium alginate oxide/GelMA hydrogel is a competitive wound dressing that can improve full-thickness infected skin defect by improving antibacterial abilities, collagen deposition, and vascularization [20]. However, the poor inherent antibacterial property of Gel-based hydrogel dressing severely hinders its application in treating infected wound healing.

Mussel-inspired chemistry relies mainly on the adhesion of dopamine to various materials and surfaces [21]. 3, 4-dihydroxy-L-phenylalanine (DOPA) is considered to be the key component of mussel adhesive proteins [22]. Dopamine (DA) belongs to a DOPA derivative with a molecular structure that is similar to that of DOPA, and it has been widely employed to modify almost all types of inorganic and organic materials substrates. Especially, DA consists of many functional groups (such as catechol and amines), which are prone to functionalization *via* non-covalent binding interaction, such as π-π stacking, hydrogen bonding, hydrophilic/hydrophobic effects, and coordination or chelation interactions between catechol groups and metal ions [22–24]. It was demonstrated that the multifunctional hydrogel composed of hydroxypropyl chitin/tannin and chelated with iron ions (Fe^{3+}) with strong antibacterial properties for infected wound healing [25]. Furthermore, DA-based hydrogels usually presented excellent tissue adhesion property and strong hemostatic activity, due to the Michael addition/Schiff base reaction between catechol groups and amino/thiol group of the tissues [26]. Hence, the fabrication of DA-based hydrogel dressings by taking advantage of metal-catechol coordination/chelation interactions effects can be a novel strategy for infected wounds treatment.

Zinc (Zn), as an important trace element, takes part in many cellular processes (e.g., DNA synthesis, enzyme activity, mitosis, and cell proliferation) [26,27]. Moreover, collagen deposition and vascularization for wound healing are related to Zn-dependent processes [26]. It was found that zinc ions (Zn^{2+}) can improve the migration of keratinocytes and self-renovation properties in the wound healing process, which is beneficial for skin regeneration [7]. Previous study also verified that Zn^{2+} presented strong antimicrobial properties because Zn^{2+} plays a vital role in destructing the activity of the enzyme system and inhibiting amino acid metabolism and adenosine triphosphate (ATP) synthesis [26]. Additionally, the electrostatic interaction between Zn^{2+} (positively charged) and bacterial substrate (negatively charged) could destroy the bacterial cell membrane, lead to leakage of intracellular compounds (protein, DNA/RNA, ATP, etc) [28]. Furthermore, it was demonstrated that the potential antibacterial mechanism of Zn-embedded biomaterials was related to the production of reactive oxygen species (ROS) [29]. Importantly, the intracellular glutathione (GSH) level, which was usually used as an indicator for evaluation of the oxidative stress levels of the bacterial cells, will significantly decrease after exposure to the environment with Zn^{2+} [19]. Therefore, zinc may present a dual-functional effect on promoting infected wound healing by inducing skin regeneration and eradicating bacteria. However, Zn^{2+} exhibits a toxic effect at high concentrations, and the threshold concentration of Zn^{2+} was closely related to cell types [30]. Watjen et al. demonstrated that 70 μM of Zn^{2+} can cause obvious toxicity to mouse fibroblast cell line (NIH-3T3), while human lung adenocarcinoma cell line (A549) exhibited Zn^{2+} toxicity up to 600 μM [31]. Previous study revealed that 1.6 ppm of Zn^{2+} could significantly increase the cell viability and alkaline phosphatase (ALP) activity of osteoblasts, but 4.4 p.m. would to toxic effect [32]. Thus, much work still needs to be further investigated. For instance, is there an optimal concentration of Zn^{2+} as an additive for balancing the antibacterial activities and promoting effect on wound healing? How to fabricate the sustained release profiles of Zn^{2+}-based hydrogel dressings for promoting infected wound healing? etc. Besides, the composite hydrogels based on the coordination effect between Zn^{2+} and catechol groups of dopamine have not yet been widely reported for infected wound dressing, and their design remains a challenging issue.

Herein, Gel and Dopa were modified with methacrylic anhydride (MA) to gelatin methacryloyl (GelMA) and dopamine methacrylamide (DMA), respectively. Then, the GelMA and DMA were cross-linked with the free radical polymerization reaction of each other to form a composite hydrogel under ultraviolet radiation without the introduction of the cross-linking agent. Zinc ions (Zn^{2+}) were loaded to form Zn^{2+}-incorporated gelatin methacryloyl/dopamine methacrylamide (Gel@Zn) hydrogels *via* the chelation effect between Zn^{2+} and *o*-dihydroxybenzebe groups of DMA (Fig. 1A).

With the addition of Zn^{2+}, Gel was employed to the development of hydrogels to solve the poor antibacterial property. Especially, the antibacterial mechanism was consisted of reducing ATP level, generation of reactive oxygen species (ROS), and leakage of protein. Moreover, the cellular experimental results demonstrated that the Gel@Zn hydrogels

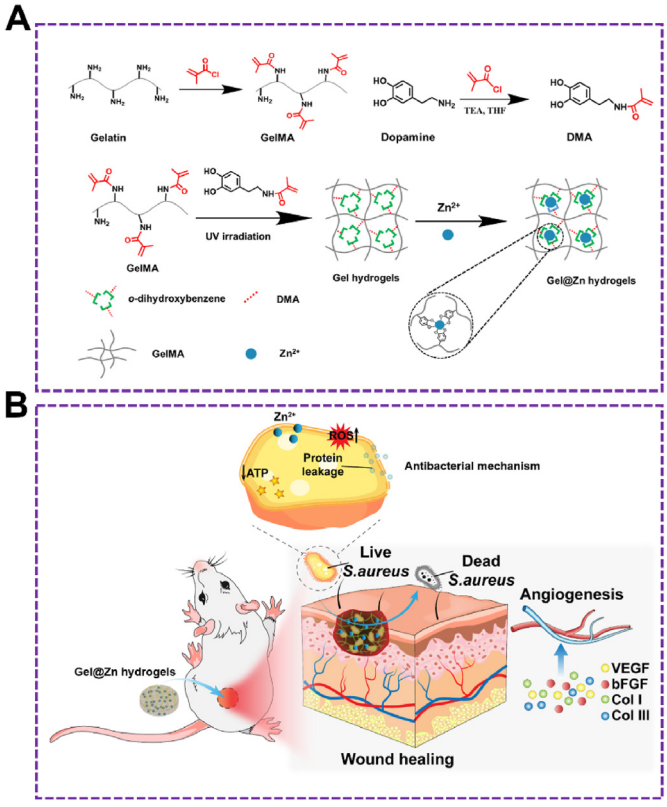

Fig. 1. (A) Synthesis of GelMA and DMA monomer and schematic illustration of the preparation of GelMA/DMA@Zn^{2+} hydrogels (Gel@Zn hydrogels). (B) Schematic illustration of Gel@Zn hydrogels for bacterial elimination to promote infected wound healing.

exhibited good biocompatibility and can improve NIH-3T3 cells migration, proliferation, and stimulate wound healing-related gene expressions. We also evaluated the mechanism of the composite hydrogel for accelerating *S. aureus*-infected wound healing and skin reconstruction by reducing the inflammatory response, enhancing antibacterial properties, inducing collagen deposition and angiogenesis activity. Hence, we speculate that the Gel@Zn hydrogel can be a promising candidate in clinical application for treating infected skin wounds.

2. Materials and methods

2.1. Materials

Geltain (Gel), dopamine (DA), zinc nitrate ($Zn(NO_3)_2$), 2-hydroxy-4'-(2-hydroxyethoxy)-2-methylpropiophenone (Irgacure 2959), and methacrylic chloride (MA) was purchased from Sigma Chemical Co. (MO, USA). CCK-8 assay kit and lactate dehydrogenase (LDH) kit were provided from Solarbio Biotechnology Co. (Beijing, China). Rhodamine–-phalloidin and Hoechst 33,258 were obtained from Invitrogen Co (USA). Fluorescein diacetate (FDA), propidium Iodide were brought from Beyotime Biotechnology Co. (Jiangsu, China). Tumor necrosis factor (TNF-α), interleukin-1β (IL-1β), interleukin-10 (IL-10), arginases-I (Arg I), and CD31 were obtained from Abcam (Shanghai, China). Other chemicals were obtained from Aladdin Industrial Co. Ltd. (Shanghai, China).

2.2. Synthesis of methacrylated-modified gelatin (GelMA)

Methacrylated-modified gelatin was synthesized according to our previous study [33]. Briefly, 5.0 g of gelatin (porcine skin type A) was dissolved in 200 mL PBS solution (0.01 M, pH 7.4) at 40 °C under vigorously stirred conditions. Following this, methacrylic chloride (20%, v/v) was added dropwise into the above gelatin solution. After reaction for 12 h, warm PBS solution (40 °C) was poured into the mixture to dilute and stop this reaction. Next, the Gel-MA mixture was dialyzed against distilled water for 5 days at 40 °C to remove the methacrylic acid and salts. Lastly, the Gel-MA solution was lyophilized for 2 days to generate white product *via* freeze drier and stored at −20 °C until further use.

2.3. Synthesis of dopamine methacrylamide (DMA)

DMA was synthesized with the reaction of amino groups from dopamine and acyl chloride groups of MA [12]. Briefly, 2.0 g of dopamine was firstly dissolved in dry THF solution under vigorously stirred conditions, and the diluted MA solution was added dropwise into the mixture with N_2 protection. The mixture was stirred at 40 °C, and the reaction was allowed to continue for 2 days. Following this, the THF was evaporated, subsequently added with DI water (10 mL), and the pH of the mixture was adjusted to 5.0 using hydrochloric acid (0.1 M) solution. To obtain purified products, ethyl acetate (50 mL) was added into the mixture under vigorously vortexed to remove unreacted DMA and recrystallize the targeted product. Importantly, the extraction recrystallization process was repeated triple and the final product was stored at −80 °C.

2.4. Preparation of Gel@Zn hydrogels

The GelMA (10%, w/v) and DMA (10%, w/v) monomers was dissolved in PBS solution (10 mL, pH = 7.4) at 40 °C, then added with photoinitiator (Irgacure 2959, 1%, w/v) and mixed under stirring conditions for 15 min. Following this, the mixture was transferred to a 24-well culture plate (500 μL/well) and exposed to UV light (8 W/cm^2) for 5 min. Next, zinc sulfate solutions (1 mL) with certain concentrations (0.04, 0.08, and 0.16 mg/mL) was added to each well. The hydrogel was soaked with Zn^{2+} solution for 6 h at room temperature. Lastly, each well was washed triple with PBS (1 mL) and the samples were denoted as Gel@Zn-0.04, Gel@Zn-0.08, and Gel@Zn-0.16, respectively. Additionally, the bare hydrogels (without Zn^{2+}) followed a procedure similar to that of Gel@Zn hydrogels.

2.5. Characterization

GelMA and DMA monomer was monitored with a nuclear magnetic resonance (^{1}HNMR) spectrometer (AVANCE500MHz, Bruker, Switzerland). Scanning electron microscopy (Quattro S, ThermoFisher Scientific, USA) was used to observe the structure of various hydrogels. The Zn content released from Gel@Zn-0.04, Gel@Zn-0.08, and Gel@Zn-0.16 was detected using coupled plasma-atomic emission spectrometer (ICP-AES, iCAP 6300 Duo, ThermoFisher Scientific, USA).

2.6. Swelling ratio evaluation

The swelling ratio of Gel, Gel@Zn-0.04, Gel@Zn-0.08, and Gel@Zn-0.16 hydrogels were assessed to determine the hold water stability. The various wet hydrogel samples were placed into 1 mL PBS solution (pH = 7.4) at 37 °C. After culturing for 12 and 24 h, various hydrogels were taken out and the superficial water was removed *via* filter paper. Finally, the hydrogels were weighted and the swelling ratio calculated with the following formula:

$$\text{Swelling ratio } (\%) = W_s/W_i \times 100\%$$

where W_s and W_i indicated the initial weight and the wet hydrogels under swelling equilibrium at 12 and 24 h.

2.7. wt loss assessment

The residual weight of the Gel, Gel@Zn-0.04, Gel@Zn-0.08, and Gel@Zn-0.16 hydrogels was measured by incubating them in PBS solution at 37 °C. In the pre-designed time point, the remaining hydrogels were taken out and the superficial water gently removed. Next, the hydrogel samples were lyophilized and weighted. Lastly, the degradation ratio of each sample was calculated based on the following formula:

$$\text{Degradation ratio } (\%) = (M_t - M_i)/M_i \times 100\%$$

where M_i is the weight of the initial hydrogel samples, and M_t is the weight of the hydrogel samples at 1 day.

2.8. Evaluation of Zn^{2+} release

To investigate the release profiles of Zn^{2+} from Gel@Zn-0.04, Gel@Zn-0.08, and Gel@Zn-0.16 hydrogels, the samples were submerged in PBS solution (5 mL) and kept at 37 °C for 0.5, 1, 3, 5, 7, 9, and 14 days. The supernatant solution was collected and then the concentrations of released Zn^{2+} were measured ICP-AES [28].

2.9. Cell experiments

2.9.1. Cell culture

NIH-3T3 fibroblast cells and RAW 264.7 were kindly provided from Chinese Academy of Sciences Cell Bank (Shanghai, China). NIH-3T3 and RAW264.7 cells were cultured with DMEM (high glucose) and supplemented with FBS (10%, v/v) and penicillin/streptomycin (1%, v/v) under 5% CO_2 atmosphere at 37 °C.

2.10. Cell morphology

The morphology of NIH-3T3 cultured with various hydrogels (thickness: 2 mm; diameter: 10 mm) was evaluated with fluorescence staining. Briefly, hydrogel samples were incubated with NIH-3T3 cells (1.0×10^4 cells/cm^2) for 2 days. Next, the cells were washed with PBS twice, fixed with 4% paraformaldehyde, permeabilized with 0.2% Triton X-100, and

stained with Rhodamine–phalloidin for cytoskeleton (red) and Hoechst 33,258 for cell nuclei (blue), respectively. Lastly, the stained cells were observed using a fluorescence microscope (Leica AF6000, Germany).

2.11. Live/dead staining

The Gel, Gel@Zn-0.04, Gel@Zn-0.08, and Gel@Zn-0.16 hydrogels (diameter: 10 mm; thickness: 2 mm) were sterilized by 75% for 20 min and they were exposed to UV light for 2 h. After that, the hydrogels were cultured with NIH-3T3 cells (1×10^5 cells/well) in 24-well plastic culture plates. After incubation of 1 and 3 days, the cells were rinsed with PBS solution and stained with FDA/PI solution in the dark for 10 min. Lastly, the stained cells were observed *via* a fluorescence microscope (Leica AF6000, Germany).

2.12. Cell proliferation

The biocompatibility of various hydrogels was tested with live/dead staining, lactate dehydrogenase (LDH) activity, and CCK-8 assay [28]. After cultured for 1 and 3 days, NIH-3T3 cells were washed with PBS twice, immediately stained FDA (10 μg/mL) and PI (10 μg/mL) solution, and then observed *via* a fluorescence microscope (Leica AF6000, Germany). For LDH activity, the cultured medium was removed from all samples after centrifugation (5000 rpm, 5 min). Next, lysis buffer (200 μL) and LDH solution (100 μL) were added to each well, followed by culturing at 37 °C for 1 h. Lastly, the OD value of the treated mixture was measured at 490 nm using a spectrophotometric microplate reader. For the CCK-8 assay, after incubation for 1 and 3 days, the cultured medium was discarded and an aliquot of prepared CCK-8 solution (40 μL) with fresh culture medium (360 μL) was added to each well. After incubation for 2 h, the optical density (OD) of the mixture was detected at 450 nm by a spectrophotometric microplate reader (BioRad 680, USA).

2.12.1. In vitro scratch test

To evaluate the effect of Gel@Zn hydrogels on the *in vitro* migration of NIH-3T3, a wound healing migration assay was performed according to our previous study [33]. After the confluence of NIH-3T3 was reached approximately 90%, a straight scratch was fabricated *via* a p20 pipette tip. The treated cells were cultured with a low FBS medium (1%, v/v) after being gently rinsed thrice by PBS to remove the cell debris. Next, the culture medium was replaced by ions containing extract culture medium. After incubation for 0 and 24 h, the cells were rinsed PBS and stained with FDA for 10 min. Lastly, images were recorded using a digital camera and quantitatively analyzed by ImageJ software to investigate the migration ratio (%) based on the following equation:

$$\text{Relative wound area } (\%) = A_t/A_0 \times 100\%$$

Therein, A_0 and A_t represent the initial scratch area (A_0) and the healed scratch area (A_h) after 24 h incubation.

2.13. Hemolytic activity evaluation

Hemolysis activity assay of the designed hydrogels was performed based on the previous study [26]. The obtained erythrocytes from the mice blood were separated by centrifugation (2000 rpm, 5 min), then washed with PBS (7.4) thrice and diluted to the final concentration of 5% (v/v). Next, 500 μL erythrocytes were added to each hydrogel sample (500 μL) in a 24-well culture plate and slightly shaken (120 rpm, 60 min) at 37 °C. Afterward, the treated mixture was collected by centrifugation (2000 rpm, 5 min) and the supernatant (200 μL) was measured with a spectrophotometric microplate reader at 540 nm. Importantly, the PBS and 0.1 Triton X-100 were employed as the negative and positive control, respectively. Lastly, the hemolysis percentage was calculated according to the following formula: Hemolysis (%) = [(Aa–Ab)/(Ac–Ab)] × 100%, where Aa was the absorbance value in the experimental groups (Gel, Gel@Zn-0.04, Gel@Zn-0.08, and Gel@Zn-0.16). Ab and Ac was the absorbance value for the Triton X-100 and PBS.

2.14. PCR analysis

To investigate the expression levels of wound healing-related genes (VEGF, bFGF, Col I, and Col III) in NIH-3T3 cells, real-time quantitative polymerase chain reaction (RT-qPCR) was employed. In brief, NIH-3T3 were cultured in 6-well culture plates (5×10^4 cells/well) with a normal culture medium. After incubation for 24 h, the culture medium was replaced by ions containing extract culture medium. The total RNA was extracted from NIH-3T3 cells by Total RNA Extract kit (Omega, China) and the concentration of total RNA was determined by a Nano-Drop One reader (Thermo Scientific, USA) after culturing for 2 and 5 days. A PrimeScript RT Master Mix reagent kit (Takara, Japan) was employed to synthesize cDNA. The GAPDH was performed as a reference and the sequences primers (Sangon, China) were exhibited in Table S1.

2.15. RAW264.7 cells response to Gel@Zn hydrogels

RAW264.7 cells were treated with LPS (25 ng/mL) as an inflammatory stimulus and then incubated with the Gel, Gel@Zn-0.04, Gel@Zn-0.08, and Gel@Zn-0.16 hydrogels for 2 days. The genes expression of TNF-α, IL-1β, IL-10, and Arg I was tested by PCR analysis. The primers (Sangon, China) used in this study were exhibited in Table S2.

2.16. Antibacterial assays

2.16.1. Antibacterial evaluation

E. coli (ATCC25922) and *S. aureus* (ATCC29213) were purchased from ATCC and cultured in Luria-Bertani (LB) culture medium. The concentration of bacteria was measured with optical density (OD) at $\lambda = 600$ nm ($OD_{600} = 0.5$ equivalent to 5.0×10^8 cells/mL). Briefly, 1 mL of *E. coli*, and *S. aureus* (1×10^6 cells/mL) were seeded on different hydrogels. After incubation of 24 h, the culture medium was discarded and the hydrogels were rinsed with aseptic PBS solution thrice to remove non-adherent bacteria. Next, bacteria were dispersed into sterile PBS solution *via* vigorous sonication (5 min). The treated bacterial suspension was then serial diluted (10,000 ×) and 200 μL of the diluted bacterial suspension was spread evenly onto LB solid plates. After incubation for 2 days, the formative colony-forming units (CFUs) of various groups were captured and counted by a digital camera. Lastly, the antibacterial ratio was calculated according to the following formula: A = (B − C)/B × 100%, in which A reveals antibacterial ratio; B is the average CFU of Gel; and C is the average CFU of Gel@Zn-0.04, Gel@Zn-0.08, and Gel@Zn-0.16 hydrogels.

Furthermore, the bacterial viabilities in the culture medium were investigated with OD_{600} values measurement. Briefly, 1 mL of *E. coli*, and *S. aureus* (1×10^6 cells/mL) were seeded on different hydrogels. After incubation for 6 and 24 h, the bacteria suspensions were diluted 1000 times and measured with the OD at $\lambda = 600$ nm.

2.17. ROS level, membrane permeability assay, BCA leakage, and ATP level

For the intracellular ROS levels of *E. coli* and *S. aureus*, the bacteria were incubated with 2′, 7′-dichlorofluorescein diacetate (DCFH-DA, 0.5 mL, 10 μM). After incubation of 0.5 h, the fluorescence intensity (FI) of each group was tested using a fluorescence spectrophotometer (λEx = 488 nm, λEm 535 nm, RF5301PC, Shimadzu, Japan). Afterward, the permeability of bacterial envelopes was evaluated with the NPN uptake assay. The *E. coli* and *S. aureus* suspension containing Gel, Gel@Zn-0.04, Gel@Zn-0.08, or Gel@Zn-0.16 were centrifuged (4000 rpm, 4 min) and incubated with NPN solution (10 μL, 10 μM). After culturing for 15 min, the FL was measured using a fluorescence spectrophotometer (λEx = 350 nm, λEm = 420 nm). Meanwhile, *E. coli* or *S. aureus* suspension incubated

with polymyxin B (PMB) was used as a positive control. For *E. coli* and *S. aureus* protein leakage, the bacterial supernatant was collected via centrifugation, added in a 96-well plate, and measured with an enhanced BCA protein assay kit. For ATP level, the bacterial suspension (1×10^6 CFU/mL) was cultured with Gel, Gel@Zn-0.04, Gel@Zn-0.08, and Gel@Zn-0.16. After culturing for 6 h, the concentration of ATP level was determined according to the Enhanced ATP Assay Kit (Beyotime, China).

2.18. Co-culture of S. aureus and NIH-3T3 cells

The NIH-3T3 cells (2×10^4 cells/mL) and *S. aureus* suspension (5×10^3 cells/mL) were seeded together with Gel, Gel@Zn-0.04, Gel@Zn-0.08, and Gel@Zn-0.16 samples. The NIH-3T3 cells viability was measured with LDH assay kit [33]. The method was referred to section 2.9.4.

2.19. Animal experiments

2.19.1. Establishment of S. aureus infectious wound healing model

Sprague Dawley (SD) mice (180–200 g) were used to perform a *S. aureus*-infected full-thickness skin defect model [2]. Briefly, pentobarbital sodium salt (1 mL/kg) was injected intraperitoneally into the mice. After the dorsal region of the mice was shaved and disinfected, the full-thickness skin wounds on the left-and-right back were created with a diameter of 10 mm through a skin needle biopsy punch. Then, 10 μL of *S. aureus* suspension (1.0×10^7 CFU/mL) were injected into the wound sites. After infection for 2 days, 30 mice were randomly divided into three groups: Control, 3 M (3 M Tegaderm ™ Film, 3662CU, 5 cm × 7 cm, Shanghai, China), and Gel@Zn-0.08. On days 0, 3, 7, and 14 after surgery, to observe the infection, the size and changes of the mice wound were recorded *via* a digital camera, and the wound contraction (%) was calculated based on the following formula:

$$\text{Wound contraction } (\%) = [(A_0\text{-}A_t)/A_0] \times 100\%$$

Where A_0 indicates the initial wound area (day 0), and A_t was the wound healing at the time, such as days 3, 7, and 14.

2.19.2. In vivo antibacterial evaluation

To assess the antibacterial effect *in vivo*, the mice were euthanized *via* inhalant anesthetic on the 1 day after surgery. Then, the exudates and pus of infected tissue in the wound sites were collected and incubated in LB broth for 24 h. After homogenization for 10 min, the suspensions were diluted (10000x) and spread onto LB agar plate to visualize the residual bacterial count.

2.19.3. Histological analysis

At 3, 7, and 14 days after surgery, the mice were euthanized in different groups and the wound tissue was collected and fixed with formaldehyde solution (10%). Then, the harvested tissues were dehydrated with graded ethanol, embedded in paraffin, and sectioned to 5 μm sections *via* Leica SP1600 Microtome (Leica, Hamburg, Germany). Next, part of the sections was treated with hematoxylin and eosin (H&E), and Masson's trichrome staining to assess the degree of inflammatory response, vascularization, and collagen deposition. Furthermore, immunohistochemistry staining of some slices was performed with rabbit polyclonal antibodies TNF-α (M1 marker), IL-1β (M1 marker), IL-10 (M2 marker), and CD31 (vascular marker) and incubated with a second antibody to observe the inflammatory response and angiogenesis in the wound sites. After that, those stained slices were visualized using a fluorescence microscope (Leica, Germany). And, the percentage of neutrophils (%) and collagen deposition (%) were obtained in the corresponding H&E stained images. Meanwhile, the quantification analysis of the immunohistochemistry staining sample was conducted *via* Image J software by counting 6 randomly selected fields. Lastly, the major organs of mice in those three groups were collected and analyzed with H&E staining for toxicology evaluation.

2.20. Statistical analysis

All of the data were exhibited as mean ± standard deviation (SD). The data were analyzed with OriginPro 8.0 for statistical analysis *via* Student's t-test and one-way analysis of variance (ANOVA). Value of * ($p < 0.05$) were considered statistically significance.

3. Results and discussions

3.1. Synthesis and characterization of GelMA and DMA

The chemical structure and synthetic route of GelMA, DMA, and the preparation process of were Gel@Zn hydrogel was shown in Fig. 1. The chemical structures of GelMA were detected by ^{1}HNMR (Fig. 2A). Compared with bare gelatin, GelMA exhibited three additional peaks (methylene, $\delta = 5.40$ and 5.65 ppm and methyl peak, $\delta = 1.91$ ppm), which ascribed to the introduction of methacrylic anhydride into gelatin molecules [33]. Besides, the degree of methacrylation of gelatin was also quantified by comparing methacrylate groups with aromatic amino acid residues of gelatin. Hence, it was revealed that GelMA was successfully prepared and the methacrylation of gelatin corresponded to

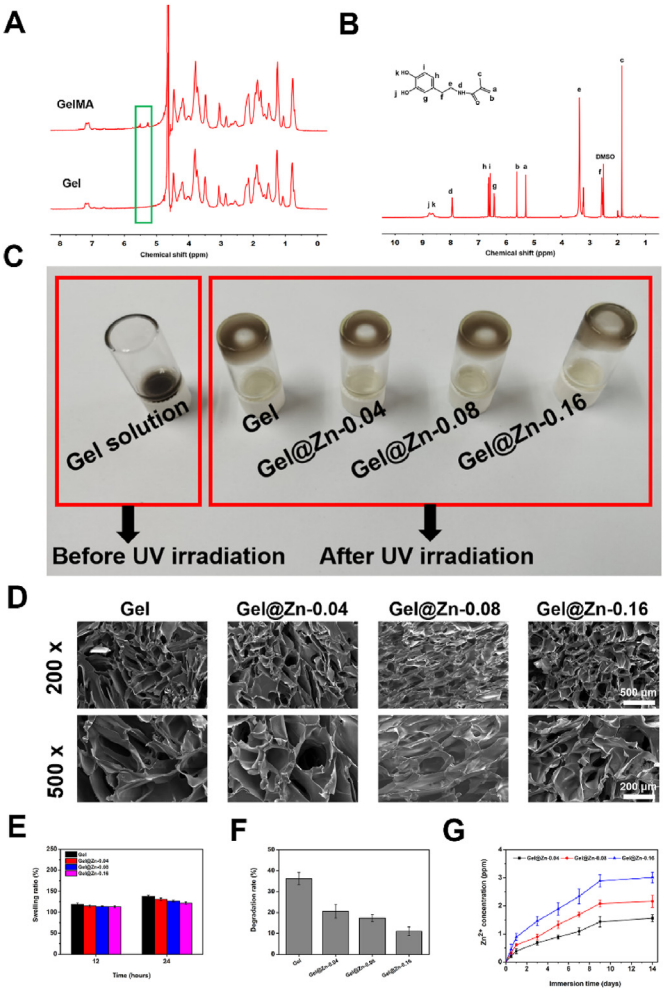

Fig. 2. The ^{1}HNMR analysis of GelMA and DMA (A & B). (C) Optical photographs of the Gel before (left) and after (right) UV irradiation and soaked with Zn^{2+} solution. (D) Scanning electron images of Gel and Gel@Zn hydrogels, scale bar: 100 μm. (E) Swelling and (F) degradation rate of Gel, Gel@Zn-0.04, Gel@Zn-0.08 and Gel@Zn-0.16 hydrogels (n = 6). (G) Controlled release of Zn^{2+} in Gel@Zn-0.04, Gel@Zn-0.08, and Gel@Zn-0.16 hydrogels.

approximately 65% based on ^{1}HNMR analysis according to our previous studies [33]. In ^{1}HNMR of DMA (Fig. 2B), new characteristic signals can be found at 5.3–5.7, 7.5, and 8.5–9.0 ppm, attributing to the two protons of acrylamide double bond, benzene ring, and phenolic hydroxyl groups [8]. These results indicated the successful modification of gelatin and dopamine molecules.

3.2. Preparation and characterization of the Zn-incorporated hydrogels

To analyze function groups of the hydrogel compared with hydrogel precursor, the ^{1}HNMR and XPS were used, respectively. As shown in Fig. S1A, compared with hydrogel precursor, two protons of acrylate double bond from GelMA and acrylamide double bond from DMA was disappeared after UV irradiation, indicated the free radical polymerization reaction was occurred. To further confirm the formation of metal coordination bonds between Zn^{2+} and the phenolic hydroxyl group of DMA molecules, the Zn 2p3 high-resolution spectrum of Gel@Zn-0.08 hydrogel was further studied (Fig. S1B). There are two kinds of coordination (Zn–O at 1021.9 eV and Zn–N at 1022.3 eV) were found (Fig. S1C), which indicated that metal coordination bonds between Zn^{2+} and the phenolic hydroxyl groups of DMA molecules were formed. As shown in Fig. 2C, the precursor Gel solution (left) was prepared by homogeneously mixing GelMA and DMA solutions at room temperature. After exposing to 365 nm UV light and soaking with Zn^{2+} solution, Gel, Gel@Zn-0.04, Gel@Zn-0.08, and Gel@Zn-0.16 hydrogels (right) was obtained based on the covalent bonds and metal coordination bonds. It can be observed that the hydrogels presented the interconnected, porous rough surface and 3D structure after freeze-dried (Fig. 2D). Meanwhile, all the hydrogels presented similar pore sizes, and the average pore size of Gel, Gel@Zn-0.04, Gel@Zn-0.08, and Gel@Zn-0.16 hydrogels decreased obviously with the content of Zn^{2+} increased. Specifically, the average pore size of above-mentioned hydrogels was 135.2 ± 17.8 μm, 118.3 ± 11.2 μm, 105.6 ± 12.4 μm, and 95.7 ± 12.6 μm, respectively (Fig. S2), which indicated that the coordination interaction between Zn^{2+} and catechol group of DMA would increase the degree of cross-linking of the hydrogels [26]. The mechanical property of the hydrogels depending on various Zn^{2+} solution concentrations was measured according to the previous study [34]. As shown in Fig. S3, with the increase in the concentration of Zn^{2+}, the Gel@Zn hydrogels exhibited a higher compressive modulus. Specifically, the compressive modulus of Gel@Zn-0.04, Gel@Zn-0.08, and Gel@Zn-0.16 hydrogels was 7.6 kPa, 9.8 kPa, and 12.4 kPa, respectively, higher than that of bare Gel hydrogel (5.9 kPa), owing to the non-covalent cross-linking network between Zn^{2+} and catechol group [26].

Previous studies revealed that the swelling and degradation ratio of the hydrogels plays a vital role in designing tissue engineering materials for cell migration, proliferation, and differentiation [3,35]. As exhibited in Fig. 2E, the swelling of the Gel hydrogels is 17.2% at 12 h. Meanwhile, when the Gel hydrogels were immersed in the Zn^{2+} solution, the swelling ratios of the Gel@Zn-0.04, Gel@Zn-0.08, and Gel@Zn-0.16 hydrogels were decreased to 14.7%, 13.5%, and 12.8%, respectively. At 24 h, the swelling ratios of the Gel, Gel@Zn-0.04, Gel@Zn-0.08, and Gel@Zn-0.16 hydrogels were 37.6%, 30.8%, 26.4%, and 21.6%. This result suggested that the existence of metal coordination bonds between Zn^{2+} and the phenolic hydroxyl groups of PDA molecules could decrease the swelling rate [26]. Additionally, the degree of swelling was decreased with increasing the concentration of Zn^{2+} for the formation of metal coordination bonds numbers. Moreover, the degree of weight loss of Gel hydrogels is higher than those of Gel@Zn hydrogels, which could be resulted from the formed metal coordination bonds that could inhibit the degradation ratio of the Gel@Zn hydrogels [34]. Specially, the degradation of Gel, Gel@Zn-0.04, Gel@Zn-0.08, and Gel@Zn-0.16 hydrogel was 36.3%, 20.6%, 17.3%, and 11.1% (Fig. 2F), respectively.

It was demonstrated that Zn^{2+} with high concentration could cause cytotoxicity to mammalian cells [32]. Hence, it was desirable to optimize the concentration of Zn^{2+} in the Gel@Zn hydrogels. The release behavior of Zn^{2+} from various Zn-incorporated hydrogels was investigated *via* ICP-AES. As shown in Fig. 2G, approximately 1.56, 2.16, and 3.01 ppm of Zn^{2+} were released from Gel@Zn-0.04, Gel@Zn-0.08, and Gel@Zn-0.16 hydrogels within 14 days, respectively. During the whole release process, it can be observed that a quick release of Zn^{2+} occurred at the first 7 days and the corresponding concentrations reached ~1.09, 1.70, and 2.34 ppm. Previous studies verified that the concentration of 2 ppm Zn^{2+} was in the safe range and presented no obvious cytotoxicity [28]. Hence, the biological properties of the prepared Gel and Gel@Zn hydrogels were further investigated.

3.3. Biocompatibility and hemocompatibility of Gel@Zn hydrogels

The cytocompatibility of the hydrogel must be taken into consideration for antibacterial wound dressings, the cell skeleton assay was performed with immunofluorescence staining [36]. The NIH-3T3 cells grown onto all hydrogel samples presented normal and spreading-out morphologies (Fig. 3A). After incubation for 24 h, the average cell spreading area on the Gel@Zn hydrogel was larger than that of the Gel hydrogel. Meanwhile, the average cell spreading area of the Gel@Zn-0.08 was higher than those of Gel@Zn-0.04 and Gel@Zn-0.16 (Fig. S4). It is demonstrated that the loading of the appropriate concentration of Zn^{2+} into GelMA/DMA hydrogel would be beneficial for NIH-3T3 cell adhesion and spreading out.

Besides, to investigate the response of Gel and Gel@Zn hydrogels (Gel@Zn-0.04, Gel@Zn-0.08, and Gel@Zn-0.16) on NIH-3T3 viability, a live/dead assay was employed (Fig. 3A). Fluorescence images confirmed that bare Gel and Gel@Zn hydrogels could not compromise NIH-3T3 survival and cellular spreading. Importantly, all most cells were stained with green fluorescence, indicated that the good biocompatibility of designed hydrogels. Furthermore, a considerable difference in NIH-3T3 intensity among all Gel@Zn hydrogels was found. Particularly, Gel@Zn-0.08 hydrogel presented a higher NIH-3T3 intensity than other hydrogels (Gel@Zn-0.04 and Gel@Zn-0.16) (Fig. S5). This phenomenon is probably ascribable to the appropriate concentration of Zn^{2+} involved in NIH-3T3 differentiation [37].

Next, the lactate dehydrogenase (LDH) assay was performed to evaluate the cytotoxicity of all hydrogel samples. The LDH, as an intracellular protein, exhibits a low level under a normal cell medium condition and could be increased considerably once cell apoptosis occurred. The quantification of LDH level was shown in Fig. 3B, the result indicated that Gel@Zn-0.04 and Gel@Zn-0.08 presented no obvious cytotoxicity for NIH-3T3 cells. However, the Gel@Zn-0.16 group displayed a slightly higher ($p < 0.05$) LDH level than Gel@Zn-0.08 samples. This suggested that the Gel@Zn-0.08 had a good cytocompatibility for antibacterial wound dressings.

Furthermore, to investigate the cell proliferation on the different hydrogels, the CCK-8 assay was performed. As shown in Fig. 3C, the NIH-3T3 cells grew and proliferated well onto all samples at 1 d and no remarkable differences were found. After incubation for 4 days, the cell viabilities of Gel@Zn hydrogels were higher ($p < 0.01$) than that of bare Gel hydrogel. Besides, the cell viability of Gel@Zn-0.08 sample was higher ($p < 0.05$) than those of the Gel@Zn-0.04 and Gel@Zn-0.16 groups. When the incubation time was prolonged to 7 days, a similar trend was obtained. Besides, a hemolysis assay was employed to further evaluate the blood compatibility of the Gel and Gel@Zn hydrogels. According to the results (Fig. S6), the positive control group was bright red. In contrast, other groups were primrose yellow and no significant difference was found. All of the above results indicated the good cytocompatibility and hemocompatibility of the Gel@Zn hydrogels.

3.4. Scratch assay

Previous studies confirmed that the inorganic metal ions (Fe^{2+}, Ca^{2+}, Sr^{2+}, Co^{2+}, and Zn^{2+} et al.) can promote cell migration for wound healing both *in vitro* and *in vivo* [37,38]. We examined the effect of Gel@Zn

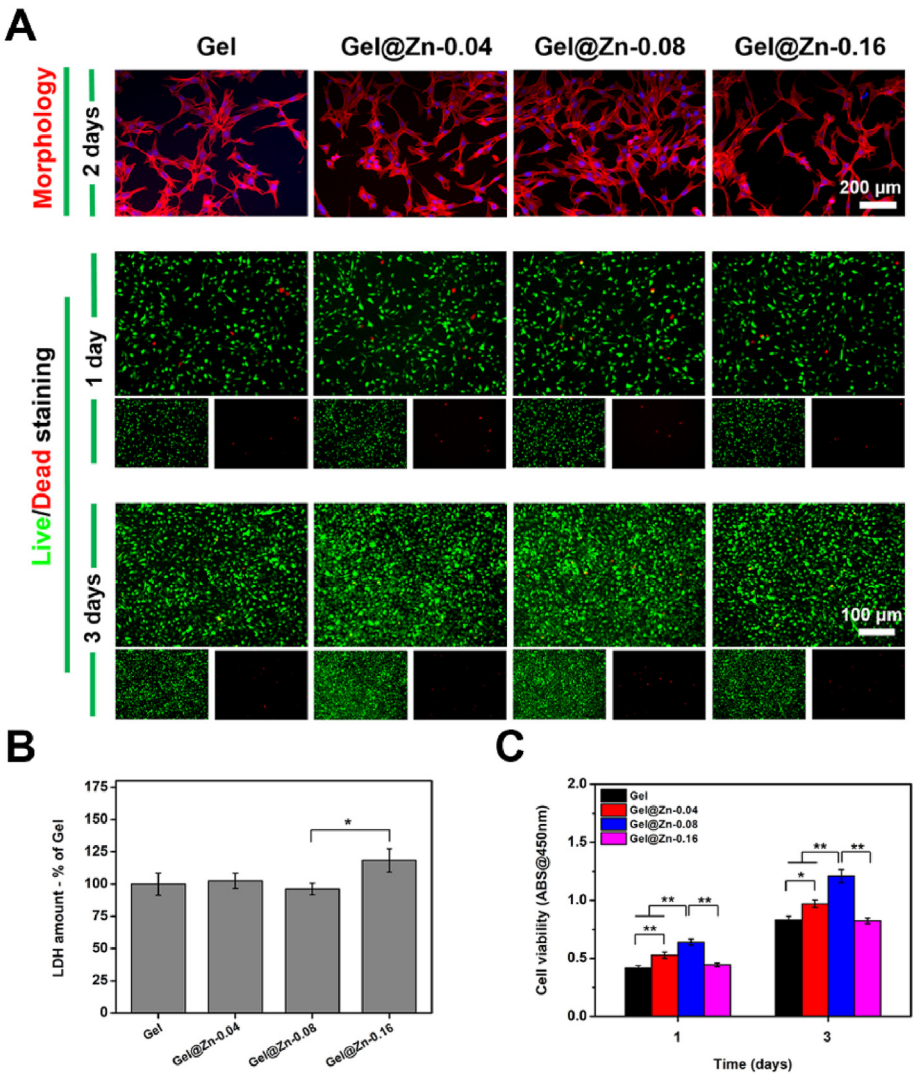

Fig. 3. (A) Cytoskeleton staining (red: actin; blue: nuclei) and live/dead fluorescent images (green: live cells, red: dead cells) of 3T3 cells after culturing with various hydrogels for 1 and 3 days. (B) LDH and (C) CCK-8 assays (n = 6), $*p < 0.05$, $**p < 0.01$. (For interpretation of the references to color in this figure legend, the reader is referred to the Web version of this article.)

hydrogels on accelerating cell migration *via* scratch assay. As shown in Fig. S7, the Gel@Zn-0.08 hydrogel effectively boosted the migration of NIH-3T3 cells and significantly ($p < 0.05$ or $p < 0.01$) expedited the wound closure compared to the Gel, Gel@Zn-0.04, Gel@Zn-0.16 groups, suggesting that the addition of appropriate concentration of Zn^{2+} could enhance the mobilization of NIH-3T3 cells.

3.5. PCR analysis

In the wound healing process, macrophages play a vital role in hemostasis, inflammation, and tissue remodeling. According to the microenvironment, macrophages could be polarized to M1 macrophages and M2 macrophages owing to their strong plasticity [39,40]. M1 macrophages secrete pro-inflammatory cytokines, including tumor necrosis factor (TNF-α) and interleukin-1β (IL-1β), which can lead to a severe inflammatory response in bacterial-infection wound healing. By comparison, M2 macrophages can alleviate inflammatory responses, improve cell migration and proliferation, angiogenesis, and skin regeneration by abundant expression of interleukin-10 (IL-10) and arginases-I (Arg I) [41]. Hence, to further characterize the macrophage polarization status, gene expressions of M1 and M2 macrophages were employed under the treatment of the Gel, Gel@Zn-0.04, Gel@Zn-0.08, and Gel@Zn-0.16 samples. According to the result, the expression of TNF-α in Gel@Zn-0.08 was significantly ($p < 0.01$) decreased as compared to Gel and Gel@Zn-0.04 groups. Additionally, a similar trend was found for IL-1β, and the expression of IL-1β in Gel@Zn-0.08 was the lowest ($p < 0.05$ or $p < 0.01$) among all groups. Moreover, the expression of M2 macrophages marker genes including IL-10 and Arg I was significantly ($p < 0.01$) elevated by the Gel@Zn-0.04, Gel@Zn-0.08, and Gel@Zn-0.16 groups compared to the control group. Importantly, the expression of IL-10 in the Gel@Zn-0.08 group was higher than those of Gel@Zn-0.04 and Gel@Zn-0.16 groups (Fig. S8). It could be concluded that the appropriate concentration of Zn^{2+} could effectively ameliorate the pro-inflammatory response and promote tissue regeneration *via* inducing the macrophage polarization from M1 to M2 in the LPS-stimulated environment, as described previously [42].

Previous studies confirmed that the appropriate concentration of Zn^{2+} presented a positive effect on enhancing the expression of wound heling-related genes [28]. Thus, we further evaluated the *in vitro* angiogenic effect of the designed hydrogels on NIH-3T3 cells. VEGF and bFGF were widely employed to reflect the angiogenic level for evaluating wound-healing effects [43]. According to the quantitative results, compared to those on other hydrogels, NIH-3T3 cells on Gel@Zn-0.08 exhibited the highest ($p < 0.05$ or $p < 0.01$) expression levels of bFGF

and VEGF (Fig. 4A and B) with culturing for 2 and 5 days. For example, the expressions of VEGF in NIH-3T3 cells on Gel@Zn-0.08 were 2.01-fold higher than that in NIH-3T3 cells group for 2 days and 1.81-fold for 5 days. It was confirmed that Zn^{2+}-based hydrogels could up-regulate the expression of Col I and Col III, which were correlated with the formation and deposition of extracellular matrix (ECM) for wound healing [43]. Hence, the gene expressions of Col I and Col III were also measured, and the results were exhibited in Fig. 4C and D. It was found that the expression levels of Col I and Col III were significantly ($p < 0.01$) increased but afterward decreased at the turning point of 0.08. In short, we could conclude that Gel@Zn-0.08 hydrogels were beneficial for suppressing the inflammatory response, improving angiogenesis level, and collagen deposition, which could be employed as wound healing dressings.

3.6. In vitro antibacterial assays

Most importantly, a desired wound healing material should present strong antibacterial properties for dealing with the bacterial infection. The inhibition effects of the various hydrogels against both *E. coli* (Gram-negative) and *S. aureus* (Gram-positive) were investigated based on the minimum inhibitory concentration (MIC) and plate coating method [3,26]. Specifically, the minimal inhibitory concentration (MIC) of Gel@Zn-0.08 hydrogel for *E. coli* and *S. aureus* was evaluated with OD_{600}. The OD value of the bacterial stock and LB culture medium was regarded as a positive and negative control [26]. As shown in Fig. S9, the MIC of Gel@Zn-0.08 hydrogel for *E. coli* and *S. aureus* were 6.0 mg/mL and 10.0 mg/mL, respectively. As presented in Fig. 5A, numerous formed CFU of *E. coli* was found in the Gel samples, and only a few residual bacteria have emerged in the Gel@Zn-0.04, Gel@Zn-0.08, and Gel@Zn-0.16 hydrogels. By quantitative analysis, the antibacterial rates of Gel@Zn-0.04 against *E. coli* were 60.2 ± 5.7% and 46.5 ± 7.6% (Fig. 5B), which could be attributed to the incorporation of Zn^{2+} presented strong antibacterial activity [34]. With the increase of Zn^{2+} concentration, the antibacterial efficiency of Gel@Zn-0.08 and Gel@Zn-0.16 hydrogels against *E. coli* were significantly increased ($p < 0.01$) compared with Gel and Gel@Zn-0.04 groups. Particularly, the antibacterial ratios of Gel@Zn-0.08 and Gel@Zn-0.16 hydrogels for *E. coli* reached 95.7 ± 4.6% and 98.6 ± 3.7%, respectively (Fig. 5B). Interestingly, no statistical difference was observed between Gel@Zn-0.08 and Gel@Zn-0.16 groups, which suggested that the releasing of Zn^{2+} from Gel@Zn-0.08 hydrogels reached the antimicrobial peak concentration, and the antibacterial abilities might not enhance along with the concentration of Zn^{2+} increased in the Gel@Zn-0.16 hydrogels [30]. Similar results were also found using *S. aureus* (Fig. 5A and C), indicating the designed hydrogel was effectively eliminating both Gram-negative and positive bacteria.

Besides, the bacterial viability in the cultured medium was also evaluated after incubated for 6 and 24 h *via* MTT assay according to our previous study. As shown in Figs. S10A and B, the bacterial viabilities of Gel@Zn-0.04, Gel@Zn-0.08, and Gel@Zn-0.16 groups were significantly lower ($p < 0.01$) than Gel group. Meanwhile, a statistical difference ($p < 0.01$) was found between Gel@Zn-0.04 and Gel@Zn-0.08 hydrogels, and no remarkable difference was observed between Gel@Zn-0.08 and Gel@Zn-0.16 groups. Collectively, these results demonstrated that the incorporation of Zn^{2+} in the hydrogels effectively kills both *E. coli* and *S. aureus*. Moreover, according to the co-culture experiment, suggested that the viability of NIH-3T3 cells in Gel@Zn-0.08 and Gel@Zn-0.16 groups was higher ($p < 0.01$) than other groups (Fig. S11). It was demonstrated that the sustained released Zn^{2+} presented the excellent antibacterial ability and good biocompatibility.

3.7. Antibacterial pathways exploration

Previous studies validated that the antibacterial pathway of Zn-incorporated biomaterials with strong anti-microbial activity was ascribed to the release of Zn^{2+} or the generation of reactive oxygen species (ROS) [30,33]. Hence, the intracellular ROS levels of *E. coli* and *S. aureus* on different samples were evaluated based on the DCFH-DA probe. As shown in Fig. 5D, the ROS levels of *E. coli* gathered in the Gel@Zn-0.04, Gel@Zn-0.08, and Gel@Zn-0.16 groups were increased to

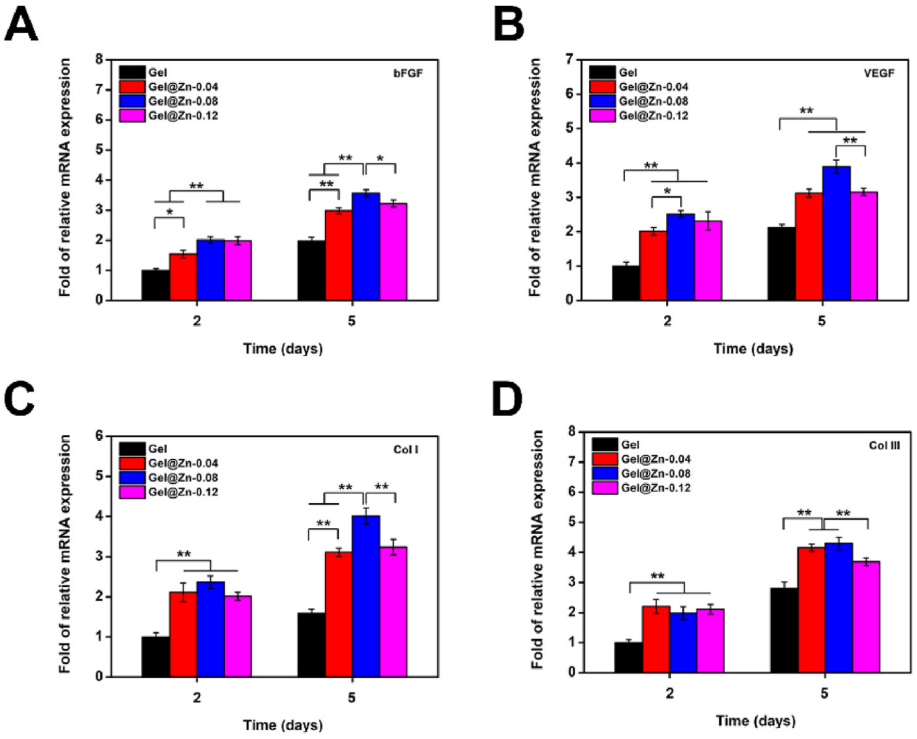

Fig. 4. PCR analysis of the genes expression related to wound healing. (A) bFGF, (B) VEGF, (C) Col I, and (D) Col III of NIH-3T3 cells. The values were normalized to GAPDH (n = 3) $*p < 0.05$, $**p < 0.01$.

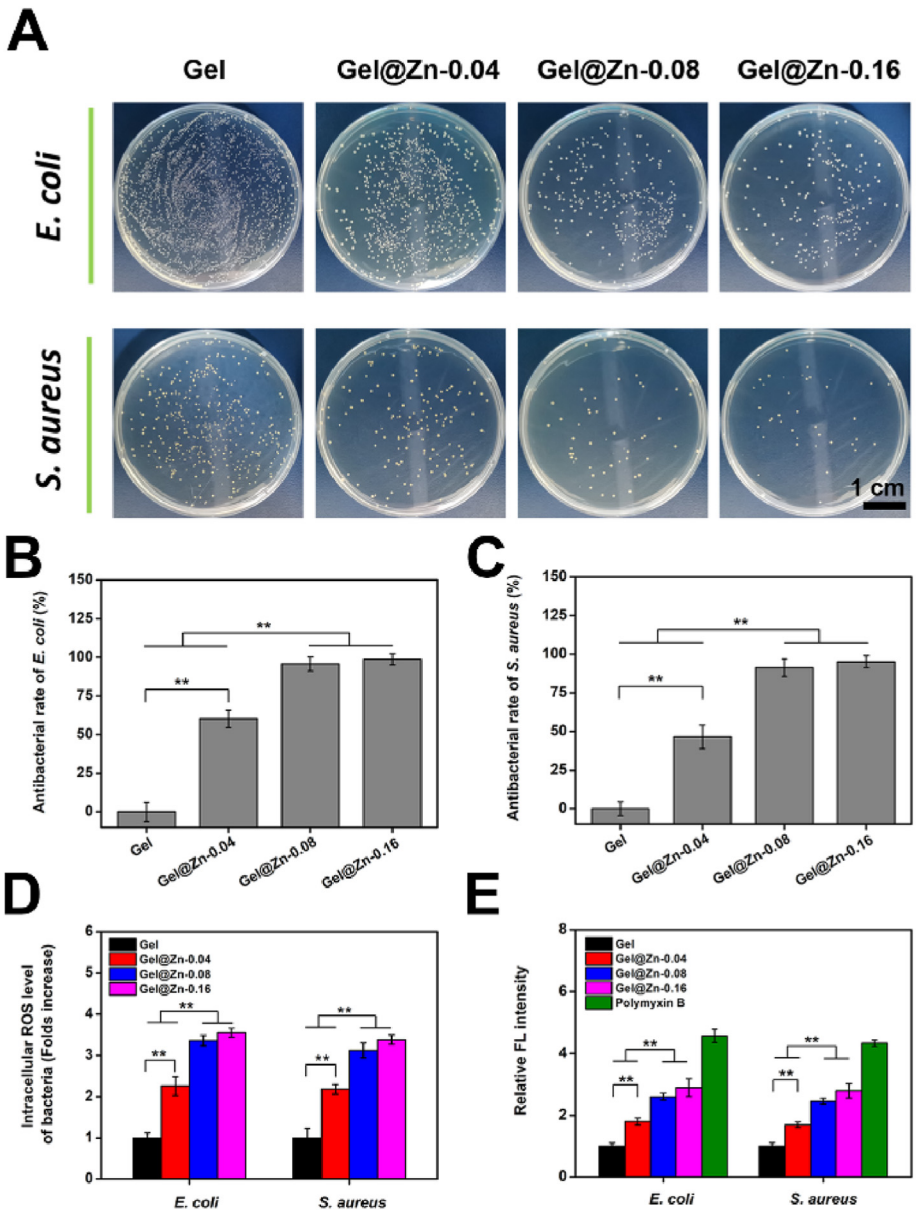

Fig. 5. (A) Photographs of *E. coli* and *S. aureus* colonies after culturing with various hydrogels. The relevant antibacterial ratios against (B) *E. coli* and (C) *S. aureus*. (D) The intracellular reactive oxygen species (ROS) of *E. coli* and *S. aureus*. (E) Bacterial envelope permeability assays using NPN staining. The final result was normalized against of Ti group. Error bars represent mean ± SD for n = 6, $*p < 0.05$, $**p < 0.01$.

2.3, 3.4, and 3.6-folds against to Gel group, respectively. Importantly, a similar result was found for *S. aureus*, revealing that the incorporation of Zn^{2+} into the hydrogel could eliminate the bacteria with the production of ROS. It was demonstrated that NPN is a small molecule (219 Da), which cannot effectively cross the outer membrane of bacteria. Once the bacterial membrane permeability was changed, it can bind to phospholipids and present strong fluorescence intensity [44]. By contrast, the fluoresces intensity of the NPN probe in an aqueous solution is weak, thus, it can be exploited to reveal the permeability of the bacterial membrane. As exhibited in Fig. 5E, the relative fluorescence (FL) intensity in the Gel@Zn-0.08 and Gel@Zn-0.16 groups were remarkably upregulated ($p < 0.01$) compared to Gel@Zn-0.04 and Gel groups. Besides, no statistical difference was found between the Gel@Zn-0.08 and Gel@Zn-0.16 groups. Once the permeability of the bacterial membrane was changed, the leakage of cellular components, such as protein and adenosine triphosphate (ATP), could be occurred [45,46]. As shown in Fig. S12, the highest increase in protein leakage was observed in Gel@Zn-0.16, corresponding to the antibacterial efficiency in Fig. 5A–C. Importantly, no significant difference was found between Gel@Zn-0.08 and Gel@Zn-0.16 groups. The concentration of ATP presented an opposed trend to that of protein leakage in *E. coli* and *S. aureus*, due to the strong antibacterial effect of Gel@Zn hydrogels on increasing a large amount of ATP leakage (Fig. S13). Collectively, these results demonstrated that the incorporation of Zn^{2+} into the hydrogel could induce ROS generation, change bacterial membrane permeability, cause protein leakage, and finally result in bacteria death.

3.8. In vivo wound healing study

Compared to Gel-Zn-0.04 and Gel-Zn-0.16 hydrogels, the Gel-Zn-0.08 hydrogel exhibited good biocompatibility, excellent hemostatic property, and strong antibacterial ability. Therefore, we selected the Gel-Zn-0.08 hydrogel as the experimental group to demonstrate the efficacy of treatment for infectious wound healing. Meanwhile, the untreated infectious wounds were used as the control groups, and the wounds covered with 3 M wound dressings were employed as the commercial

groups [43]. As shown in Fig. 6A, the photographs of the wound sites in these three groups were imaged with a digital camera on day 0, 3, 7, and 14 according to our previous study [43]. Importantly, the efficiency of wound healing was evaluated based on a comparison of wound site during the wound healing process with that of original wound issues at day 0. On day 3 and 7, the wound areas of 3 M and Gel@Zn-0.08 were significantly smaller ($p < 0.05$ or $p < 0.01$) than the control group. Notably, the wounds treated with Gel@Zn-0.08 presented the highest wound closure compared to control and 3 M groups on day 3 and 7 ($p < 0.01$). Prolonged to 14 days, a similar trend was found and the percentage of wound contraction of control, 3 M, and Gel@Zn-0.08 were reached 86.2%, 92.9%, and 98.6%, respectively (Fig. 6B). Besides, to evaluate the anti-infective property of Gel@Zn-0.08 *in vivo*, the residual *S. aureus* from wound sites on day 1 were collected and incubated in LB agar plates (Fig. 6C). It was found that the bacteria count in the Gel@Zn-0.08 group was much lower than those of the control and 3 M groups, indicating a strong antibacterial ability *in vivo*. In detail, the number of formed *S. aureus* on control, 3 M, and Gel@Zn-0.08 groups were 644 ± 85, 230 ± 53, and 73 ± 17, respectively (Fig. 6D).

Considering that collagen deposition played a vital role in accelerating infectious wound healing due to it can maintain the structure of new-formed skin, induce the formation of granulation tissue [43,47]. Previous studies revealed that the collagen was composed of hydroxyproline (HYP) and the percentage of mass reached 13.4% [47]. Therefore, the level of collagen deposition of the control, 3 M, and Gel@Zn-0.08 was evaluated based on HYP concentration. As presented in Fig. 6E, the Gel@Zn-0.08 group displayed the highest ($p < 0.01$) HYP concentration compared to the control and 3 M groups on day 3, suggesting more collagen deposition for infectious wound healing. By comparison, the lowest level of collagen deposition was found in the control group, indicating that serious bacterial infections could delay the wound healing process. Notably, a significant difference ($p < 0.01$) was found between control and 3 M groups, suggesting the commercial 3 M wound dressings had a certain therapeutic effect for infectious wound healing [43]. After treatment for 7 and 14 days, Gel@Zn-0.08 hydrogel exhibited a higher ($p < 0.01$) HYP concentration compared with the control and 3 M groups, indicated the synergistic effect of excellent anti-infective property, good biocompatibility, and released profile of Zn^{2+} were beneficial for promoting infectious wound healing.

3.9. Histological analysis of wound healing tissue

To evaluate the inflammatory responses and collagen deposition of the regenerative skin tissue after treatment with Gel@Zn-0.08 hydrogels, the histological analysis of H&E and Masson's trichrome staining was employed. As shown in Fig. 7A, after treatment for 3 and 7 days, inflammatory infiltration was observed in control and 3 M groups, suggesting severe bacterial infection remaining existed in the wound sites [43]. By contrast, only a few inflammatory infiltration was emerged in the Gel@Zn-0.08 group, indicating the excellent anti-infective ability

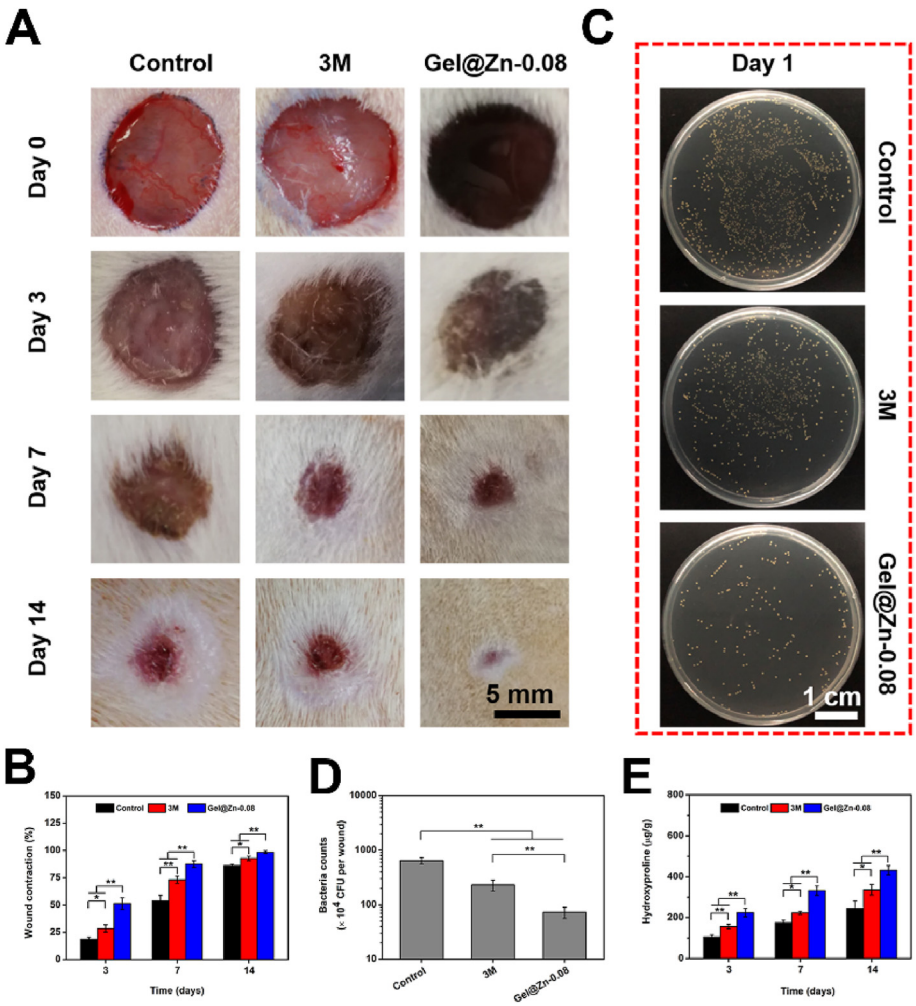

Fig. 6. (A) Gross observation of the wound at predetermined time points for control, 3 M, and Gel@Zn-0.08 groups. (B) Quantification analysis of wound closure at day 3, 7, and 14. (C) Representative images of *S. aureus* colonies survived in various groups. (D) The number of residual *S. aureus* under different conditions. (E) Quantification of collagen deposition (n = 6), *$p < 0.05$, **$p < 0.01$.

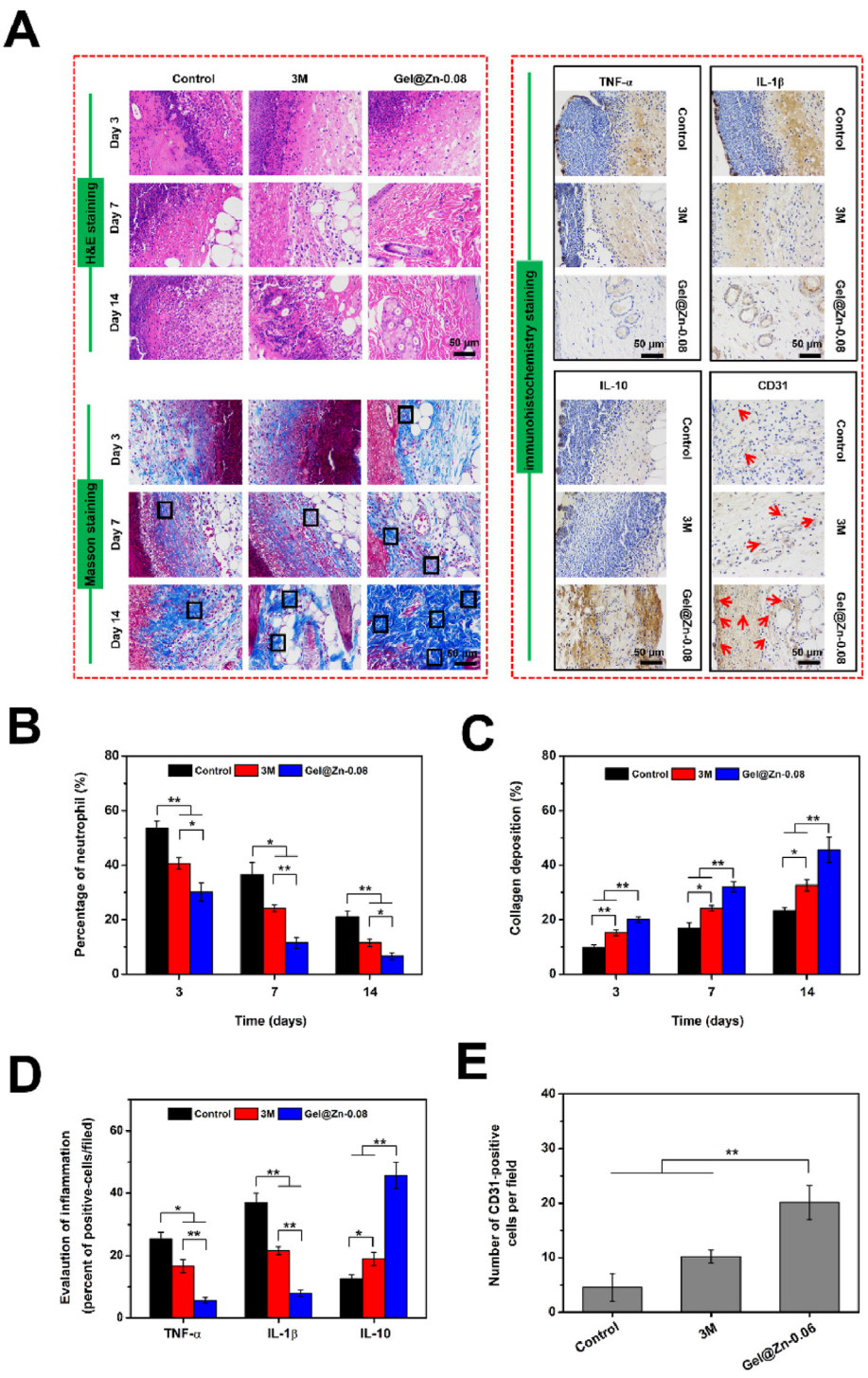

Fig. 7. (A) Histological images of the infected wound sites by H&E, Masson's trichrome and immunohistochemistry staining (newborn ordered collagen fibers: black rectangles, newly formed blood vessels: red arrows). (B) Quantification of percentage of neutrophils based on H&E staining. (C) Percentage of collagen deposition according to Masson's trichrome staining. (D) Evaluation of inflammation of TNF-α, IL-1β, and IL-10. (E) Quantitative analysis of newly formed blood vessels based on CD31 staining (n = 6), $*p < 0.05$, $**p < 0.01$. (For interpretation of the references to color in this figure legend, the reader is referred to the Web version of this article.)

could reduce the inflammatory responses resulting from bacterial infection. On day 14 of treatment, there was still inflammatory infiltration emerged in the control and 3 M groups. In comparison, the reconstruction of infectious skin had started and a large number of newly-formed and aligned collagenous structures were observed. Additionally, almost no inflammatory infiltration was found in the Gel@Zn-0.08. By quantitative analysis, the degree of inflammatory infiltration in all three groups following this sequence: Gel@Zn-0.08 < 3 M < control (Fig. 7B).

Furthermore, a previous study confirmed that neovascularization could promote collagen deposition in the regenerated skin tissue, granulation tissue formation, and accelerate infectious wound healing [48, 49]. In Fig. 7A, a large amount of newborn ordered collagen fibrils (indicated by black rectangles) were observed in Gel@Zn-0.08 group. After treatment of 7 and 14 days, more mature collagen fibrils were found in the Gel@Zn-0.08 hydrogel compared with partially new-formed collagen fibers in the control and 3 M groups (Fig. 7C). It was demonstrated that Gel@Zn-0.08 hydrogel presented a positive impact on accelerating the infectious wound healing process.

3.10. Immunohistochemistry (IHC) staining analysis

The previous studies revealed that the inflammatory response is inevitable, resulting from the internal factors (intrinsic inflammatory phase, disease, etc.) and external factors (foreign materials, bacterial

infection, etc.) [50,51]. Therefore, we selected tumor necrosis factor-α (TNF-α) and Interleukin-1β (IL-1β) as the indicators to evaluate the healing efficiency of the Gel@Zn-0.08 hydrogel. As shown in Fig. 7A and D, the expressions of TNF-α and IL-1β in the Gel@Zn-0.08 were lower ($p < 0.01$) than those of control and 3 M groups, indicating that the sustained release of Zn^{2+} from the Gel@Zn-0.08 hydrogel could eliminate the pathogens in the infectious wound issues and therefore reduce the inflammatory response. Importantly, a remarkable difference ($p < 0.05$ or $p < 0.01$) was found between control and 3 M groups, indicating the 3 M wound dressings had a positive effect on reducing the inflammatory response, but the therapeutic effect was inferior in Gel@Zn-0.08 hydrogel. Interleukin-10 (IL-10), a type of anti-inflammatory factor, plays an important role in maintaining the anti-inflammatory microenvironment and improving the wound healing process. The expression of IL-10 in Gel@Zn-0.08 group was significantly higher ($p < 0.01$) than those of the control and 3 M groups (Fig. 7A and D), revealing that the Gel@Zn-0.08 hydrogel could stimulate the expression of IL-10 to regulate and induce the anti-inflammatory microenvironment.

The formation of new blood vessels is widely associated with the re-epithelialization and could accelerate the wound healing process [52,53]. With the aid of CD31 staining (neovascularization maker), it was found that remarkably more CD31-positive cells (marked by black arrows) emerged in the Gel@Zn-0.08 group, suggesting active promoting of new capillaries formation for the wound healing process. After quantitative analysis, only a few CD31-positive cells were observed in the control and 3 M groups with expressions of $4.6 \pm 2.5\%$ and $10.2 \pm 1.2\%$, respectively. In comparison, the Gel@Zn-0.08 treated one presented significantly increased ($p < 0.01$) expression of CD31 staining, with the value of $20.1 \pm 3.1\%$ (Fig. 7E). These results verified that the Gel@Zn-0.08 could effectively eradicate the bacteria in the infectious wound sites, thus suppressing the inflammatory responses, improving collagen deposition, stimulating angiogenesis, and simultaneously accelerating infectious wound healing.

4. Conclusion

In summary, Gel, Dopa, and Zn^{2+} were employed to fabricate Gel@Zn composite hydrogels with strong antibacterial and infected wound healing-promoting properties.

The Gel@Zn hydrogels were fabricated based on the gelatin methacrylate (GelMA) and dopamine methacrylate (DMA) by free-radical polymerization and metal coordination bonds between Zn^{2+} and the phenolic hydroxyl group of dopamine methacrylate. The Gel@Zn-0.08 hydrogel presented an interconnected and porous 3D structure and exhibited a sustained release profile of Zn^{2+}. Antibacterial assays demonstrated that the Gel@Zn-0.08 hydrogels with strong antibacterial abilities against *E. coli* (Gram-negative bacteria) and *S. aureus* (Gram-positive bacteria) *via* generation of ROS and increase membrane permeability. Besides, the Gel@Zn-0.08 hydrogels with good cytocompatibility for improving the adhesion, proliferation, and migration of NIH-3T3 cells. Meanwhile, the Gel@Zn-0.08 hydrogels could stimulate wound healing-related gene expression and collagen deposition. The *in vivo* studies also demonstrated that the carbohydrates composite hydrogel could remarkably accelerate the infected wound healing process by effectively killing bacteria, suppressing the inflammatory response, improving vascularization and collagen deposition levels, and simultaneously promoting skin regeneration. Overall, this study will provide a new strategy for the development of wound dressing to promote infected wound healing.

Credit author statement

Bailong Tao: Investigation, Methodology, Data curation, Investigation, Writing – original draft. **Chuanchuan Lin**: Investigation, Data curation, Writing – original draft. **Xian Qin**: Investigation. **Yonglin Yu**: Validation. **Ai Guo**: Investigation, Formal analysis. **Kai Li**: Visualization. **Hongchuan Tian**: Investigation, Formal analysis. **Weiwei Yi**: Investigation, Formal analysis. **Dengliang Lei**: Investigation, Formal analysis. **Yue Chen**: Investigation, Formal analysis. **Ligue Chen**: Conceptualization, Supervision, Writing – original draft.

Declaration of competing interest

The authors declare that they have no known competing financial interests or personal relationships that could have appeared to influence the work reported in this paper.

Acknowledgments

This work was financially supported by National Natural Science Foundation of China (82102537, 82160411&82002278), Natural Science Foundation of Chongqing Science and Technology Commission (No. cstc2021jcyj-msxmX0170), Science and Technology Panning Project of Guizhou Province (Qiankehe Platform Talents [2017] 5733–075), Science and Technology Fund Project of Guizhou Provincial Health Commission (gzwjkj2019-1-213), the First Affiliated Hospital of Chongqing Medical University cultivating fund (PYJJ2021-02, PYJJ2021-04), the Affiliated Hospital of Zunyi Medical University PhD Research Startup Fund (2019–06), Science and Technology Panning Project of Guizhou Province (Qiankehe Basic-ZK [2021] General 388).

Appendix A. Supplementary data

Supplementary data to this article can be found online at https://doi.org/10.1016/j.mtbio.2022.100216.

References

[1] N. Annabi, D. Rana, E.S. Sani, R. Portillo-Lara, J.L. Gifford, M.M. Fares, S.M. Mithieux, A.S. Weiss, Engineering a sprayable and elastic hydrogel adhesive with antimicrobial properties for wound healing, Biomaterials 139 (2017) 229–243.
[2] W.G. Liu, M. Wang, W. Cheng, W. Niu, M. Chen, M. Luo, C.X. Xie, T.T. Leng, L. Zhang, B. Lei, Bioactive antiinflammatory antibacterial hemostatic citrate-based dressing with macrophage polarization regulation for accelerating wound healing and hair follicle neogenesis, Bioact. Mater. 6 (2011) 721–728.
[3] J. Leng, Y. He, Z. Yuan, B.L. Tao, K. Li, C.C. Lin, K. Xu, M.W. Chen, L.L. Dai, X.M. Li, T.J. Huang, K.Y. Cai, Enzymatically-degradable hydrogel coatings on titanium for bacterial infection inhibition and enhanced soft tissue compatibility via a self-adaptive strategy, Bioact. Mater. 6 (2021) 4670–4685.
[4] L. Cheng, Z.W. Cai, T.J. Ye, X.H. Yu, Z.J. Chen, Y.F. Yan, Q. Jin, L. Wang, Z.H. Liu, W.G. Cui, L.F. Deng, Injectable polypeptide-protein hydrogels for promoting infected wound healing, Adv. Funct. Mater. 30 (2020) 2001196.
[5] X.J. Yang, X.M. Sun, J. Liu, Y.R. Huang, Y.H. Peng, Y.N. Xu, L. Ren, Photo-crosslinked GelMA/collagen membrane loaded with lysozyme as an antibacterial corneal implant, Int. J. Biol. Macromol. 191 (2021) 1006–1016.
[6] G. Gao, Y.W. Jiang, H.R. Jia, F.G. Wu, Near-infrared light-controllable on-demand antibiotics release using thermo-sensitive hydrogel-based drug reservoir for combating bacterial infection, Biomaterials 188 (2019) 83–95.
[7] C.Y. Mao, Y.M. Xiang, X.M. Liu, Z.D. Cui, X.J. Yang, K.W.K. Yeung, H.B. Pan, X.B. Wang, P.K. Chu, S.L. Wu, Photo-Inspired antibacterial activity and wound healing acceleration by hydrogel embedded with Ag/Ag@AgCl/ZnO nanostructures, ACS Nano 11 (2017) 9010–9021.
[8] L. Han, X. Lu, K.Z. Liu, K.F. Wang, L.M. Fang, L.T. Weng, H.P. Zhang, Y.H. Tang, F.Z. Ren, C.C. Zhao, G.X. Sun, R. Liang, Z.J. Li, Mussel-inspired adhesive and tough hydrogel, ACS Nano 11 (2017) 2561–2574.
[9] Y. Huang, X. Zhao, C.B. Wang, J.Y. Chen, Y.Q. Liang, Z.L. Li, Y. Han, B.L. Guo, High-strength anti-bacterial composite cryogel for lethal noncompressible hemorrhage hemostasis synergistic physical hemostasis and chemical hemostasis, Chem. Eng. J. 427 (2022) 131977.
[10] Z.R. Jia, J.L. Gong, Y. Zeng, J.H. Ran, J. Liu, K.F. Wang, C.M. Xie, X. Lu, J. Wang, Bioinspired conductive silk microfiber integrated bioelectronic for diagnosis and wound healing in diabetes, Adv. Funct. Mater. 31 (2021) 2010461.
[11] A.G. Kurian, R.K. Singh, K.D. Patel, J.H. Lee, H.W. Kim, Multifunctional GelMA platforms with nanomaterials for advanced tissue therapeutics, Bioact. Mater. 8 (2022) 267–295.
[12] Q.Q. Lei, Y.W. Zhang, W.N. Zhang, R.W. Li, N.J. Ao, H. Zhang, A synergy between dopamine and electrostatically bound bactericide in a poly (vinyl alcohol) hybrid hydrogel for treating infected wounds, Carbohydr. Polym. 272 (2021) 118513.
[13] M. Li, Y.P. Liang, Y.Q. Liang, G.Y. Pan, B.L. Guo, Injectable stretchable self-healing dual dynamic network hydrogel as adhesive anti-oxidant wound dressing for photothermal clearance of bacteria and promoting wound healing of MRSA infected motion wounds, Chem. Eng. J. 427 (2022) 132039.

[14] Y.P. Liang, B.J. Chen, M. Li, J.H. He, Z.H. Yin, B.L. Guo, Injectable antimicrobial conductive hydrogels for wound disinfection and infectious wound healing, Biomacromolecules 21 (2020) 1841–1852.
[15] Y.P. Liang, J.H. He, B.L. Guo, Functional hydrogels as wound dressing to enhance wound healing, ACS Nano 15 (2021) 12687–12722.
[16] H.J. Xu, S.H. Huang, J.J. Wang, Y. Lan, L.B. Feng, M.S. Zhu, Y. Xiao, B. Cheng, W. Xue, R. Guo, Enhanced cutaneous wound healing by functional injectable thermo-sensitive chitosan-based hydrogel encapsulated human umbilical cord-mesenchymal stem cells, Int. J. Biol. Macromol. 137 (2019) 433–441.
[17] C.C. Lin, B.L. Tao, Y.M. Deng, Y. He, X.K. Shen, R. Wang, L. Lu, Z.H. Peng, Z.Z.L. Xia, K.Y. Cai, Matrix promote mesenchymal stromal cell migration with improved deformation via nuclear stiffness decrease, Biomaterials 217 (2019) 119300.
[18] F. Nazir, I. Ashraf, M. Iqbal, T. Ahmad, S. Anjum, 6-deoxy-aminocellulose derivatives embedded soft gelatin methacryloyl (GelMA) hydrogels for improved wound healing applications: in vitro and in vivo studies, Int. J. Biol. Macromol. 185 (2021) 419–433.
[19] P. Liu, Y.C. Zhao, Z. Yuan, H.Y. Ding, Y. Hu, W.H. Yang, K.Y. Cai, Construction of Zn-incorporated multilayer films to promote osteoblasts growth and reduce bacterial adhesion, Mater. Sci. Eng. C 75 (2017) 998–1005.
[20] Z.W. Deng, M.H. Li, Y. Hu, Y. He, B.L. Tao, Z. Yuan, R. Wang, M.W. Chen, Z. Luo, K.Y. Cai, Injectable biomimetic hydrogels encapsulating Gold-metal–organic-frameworks nanocomposites for enhanced antibacterial and wound healing activity under visible light actuation, Chem. Eng. J. 420 (2021) 1229668.
[21] M.S. Ma, Y.L. Zhong, X.L. Jiang, Thermosensitive and pH-responsive tannin-containing hydroxypropyl chitin hydrogel with long-lasting antibacterial activity for wound healing, Carbohydr. Polym. 236 (2020) 116096.
[22] C.Y. Mu, Y. Hu, Y.H. Hou, M.H. Li, Y. He, X.K. Shen, B.L. Tao, C.C. Lin, M.W. Chen, M.H. Chen, K.Y. Cai, Substance P-embedded multilayer on titanium substrates promotes local osseointegration via MSC recruitment, J. Mater. Chem. B 8 (2020) 1212–1222.
[23] L.J. Pruett, C.H. Jenkins, N.S. Singh, K.J. Catallo, D.R. Griffin, Heparin microislands in microporous annealed particle scaffolds for accelerated diabetic wound healing, Adv. Funct. Mater. 31 (2021) 2104337.
[24] X.L. Qi, W.H. Pan, X.Q. Tong, T. Gao, Y.J. Xiang, S.Y. You, R.T. Mao, J. Cui, R.D. Hu, W.Z. Zhang, H. Deng, J.L. Shen, ε-Polylysine-stabilized agarose polydopamine hydrogel dressings with robust photothermal property for wound healing, Carbohydr. Polym. 264 (2021) 118046.
[25] Y.N. Qian, C.C. Xu, W. Xiong, N. Jiang, Y.J. Zheng, X.J. He, F. Ding, X.H. Lu, J.L. Shen, Dual cross-linked organic-inorganic hybrid hydrogels accelerate diabetic skin wound healing, Chem. Eng. J. 417 (2021) 129335.
[26] Y.T. Yang, Y.P. Liang, J.Y. Chen, X.L. Duan, B.L. Guo, Mussel-inspired adhesive antioxidant antibacterial hemostatic composite hydrogel wound dressing via photo-polymerization for infected skin wound healing, Bioact. Mater. 8 (2022) 341–354.
[27] X.K. Shen, Y.Y. Zhang, P.P. Ma, L. Sutrisno, Z. Luo, Y. Hu, Y.L. Yu, B.L. Tao, C.Q. Li, K.Y. Cai, Fabrication of magnesium/zinc-metal organic framework on titanium implants to inhibit bacterial infection and promote bone regeneration, Biomaterials 212 (2019) 1–16.
[28] B.L. Tao, W.K. Zhao, C.C. Lin, Z. Yuan, Y. He, L. Lu, M.W. Chen, Y. Ding, Y.L. Yang, Z.Z.L. Xia, K.Y. Cai, Surface modification of titanium implants by ZIF-8@Levo/LBL coating for inhibition of bacterial-associated infection and enhancement of in vivo osseointegration, Chem. Eng. J. 390 (2020) 124621.
[29] Y.M. Xiang, X.M. Liu, C.Y. Mao, X.M. Liu, Z.D. Cui, X.J. Yang, K.W.K. Yeung, Y.F. Zheng, S.L. Wu, Infection-prevention on Ti implants by controlled drug release from folic acid/ZnO quantum dots sealed titania nanotubes, Mater. Sci. Eng. C 85 (2018) 214–224.
[30] X.K. Shen, Y. Hu, G.Q. Xu, W.Z. Chen, K. Xu, Q.C. Ran, P.P. Ma, Y.R. Zhang, J.H. Li, K.Y. Cai, Regulation of the biological functions of osteoblasts and bone formation by Zn-incorporated coating on microrough titanium, ACS Appl. Mater. Interfaces 6 (2014) 16426–16440.
[31] W. Watjen, H. Haase, M. Biagioli, D. Beyersmann, Induction of apoptosis in mammalian cells by cadmium and zinc, Environmen. Health Persp. 110 (2021) 865–867.
[32] V. Aina, A. Perardi, L. Bergandi, G. Malavasi, L. Menabue, et al., Cytotoxicity of zinccontaining bioactive glasses in contact with human osteoblasts, Chem. Biol. Interact. 167 (2007) 207–218.
[33] B.L. Tao, C.C. Lin, Y.M. Deng, Z. Yuan, X.K. Shen, M.W. Chen, Y. He, Z.H. Peng, Y. Hu, K.Y. Cai, Copper-nanoparticle-embedded hydrogel for killing bacteria and promoting wound healing with photothermal therapy, J. Mater. Chem. B 7 (2019) 2534–2548.
[34] X. Yi, J.P. He, X.L. Wang, Y. Zhang, G.X. Tan, Z.N. Zhou, J.Q. Chen, D.F. Chen, R.X. Wang, W. Tian, P. Yu, L. Zhou, C.Y. Ning, Tunable mechanical, antibacterial, and cytocompatible hydrogels based on a functionalized dual network of metal coordination bonds and covalent crosslinking, ACS Appl. Mater. Interfaces 10 (2018) 6190–6198.
[35] M.P. Tian, A.D. Zhang, Y.X. Yao, X.G. Chen, Y. Liu, Mussel-inspired adhesive and polypeptide-based antibacterial thermo-sensitive hydroxybutyl chitosan hydrogel as BMSCs 3D culture matrix for wound healing, Carbohydr. Polym. 261 (2021) 117878.
[36] G.P. Guan, Q.Z. Lv, S.Y. Liu, Z.Z. Jiang, C.X. Zhou, W.F. Liao, 3D-bioprinted peptide coupling patches for wound healing, Mater, Today Bio 13 (2022) 100188.
[37] L.L. Sheng, Z.W.B. Zhang, Y. Zhang, E.D. Wang, B. Ma, Q. Xu, L.L. Ma, M. Zhang, G. Pei, J. Chang, A novel "hot spring"-mimetic hydrogel with excellent angiogenic properties for chronic wound healing, Biomaterials 264 (2021) 120414.
[38] B.L. Tao, C.C. Lin, A. Guo, Y.L. Yu, X. Qian, K. Li, H.C. Tian, W.W. Yi, D.L. Lei, L.X. Chen, Fabrication of copper ions-substituted hydroxyapatite/polydopamine nanocomposites with high antibacterial and angiogenesis effects for promoting infected wound healing, J. Ind. Eng. Chem. 104 (2021) 345–355.
[39] Z. Yuan, C.C. Lin, L.L. Dai, Y. He, J.W. Hu, K. Xu, B.L. Tao, P. Liu, K.Y. Cai, Near-infrared light-activatable dual-action nanoparticle combats the established biofilms of methicillin-resistant *Staphylococcus aureus* and its accompanying inflammation, Small 17 (2021) 2007522.
[40] S.Q. Wang, H. Zheng, L. Zhou, F. Cheng, Z. Liu, H.P. Zhang, Q.Y. Zhang, Injectable redox and light responsive MnO_2 hybrid hydrogel for simultaneous melanoma therapy and multidrug-resistant bacteria-infected wound healing, Biomaterials 260 (2020) 120314.
[41] Z. Yuan, C.C. Lin, Y. He, B.L. Tao, M.W. Chen, J.X. Zhang, P. Liu, K.Y. Cai, Near-infrared light-triggered nitric-oxide enhanced photodynamic therapy and low temperature photothermal therapy for biofilm elimination, ACS Nano 14 (2020) 3546–3562.
[42] G.Y. Guo, T. Guo, H. Shen, Q.J. Wang, F. Jiang, J. Tang, X.W. Jiang, J.X. Wang, X.L. Zhang, W.B. Bu, Self-amplification immunomodulatory strategy for tissue regeneration in diabetes based on cytokine-ZIFs system, Adv. Funct. Mater. 31 (2021) 2100795.
[43] B.L. Tao, C.C. Lin, Z. Yuan, Y. He, M.W. Chen, K. Li, J.W. Hu, Y.L. Yang, Z.Z.L. Xia, K.Y. Cai, Near infrared light-triggered on-demand Cur release from Gel-PDA@Cur composite hydrogel for antibacterial wound healing, Chem. Eng. J. 403 (2021) 126182.
[44] B.L. Tao, C.C. Lin, Y. He, Z. Yuan, M.W. Chen, K. Xu, K. Li, A. Guo, K.Y. Cai, L.X. Chen, Osteoimmunomodulation mediating improved osteointegration by OGP-loaded cobalt-metal organic framework on titanium implants with antibacterial property, Chem. Eng. J. 423 (2021) 130176.
[45] K. Xu, Z. Yuan, Y. Ding, Y. He, K. Li, C.C. Lin, B.L. Tao, Y.L. Yu, X. Li, P. Liu, K.Y. Cai, Near-infrared light triggered multi-mode synergetic therapy for improving antibacterial and osteogenic activity of titanium implant, Appl. Mater. Today 24 (2021) 101155.
[46] Z. Yuan, B.L. Tao, Y. He, J. Liu, C.C. Lin, X.K. Shen, Y. Ding, Y.L. Yu, C.Y. Mu, P. Liu, K.Y. Cai, Remote eradication of biofilm on titanium implant via near-infrared light triggered photothermal/photodynamic therapy strategy, Biomaterials 217 (2019) 119290.
[47] M. Li, Y.P. Liang, J.H. He, H.L. Zhang, B.L. Guo, Two-pronged strategy of biomechanically active and biochemically multifunctional hydrogel wound dressing to accelerate wound closure and wound Healing, Chem. Mater. 32 (2020) 9937–9953.
[48] Y.P. Liang, Z.L. Li, Y. Huang, R. Yu, B.L. Guo, Dual-dynamic-bond cross-linked antibacterial adhesive hydrogel sealants with on-demand removability for post-wound closure and infected wound healing, ACS Nano 15 (2021) 7078–7093.
[49] Y.T. Zhang, G. Wu, L.M. CHen, Y. Zhang, Y.W. Luo, Y. Zheng, F.J. Hu, T. Forouzanfar, H.Y. Lin, B. Liu, Neuro-regenerative imidazole-functionalized GelMA hydrogel loaded with hAMSC and SDF-1α promote stem cell differentiation and repair focal brain injury, Bioact. Mater. 6 (2021) 627–637.
[50] F.F. Zhou, Y. Hong, R.J. Liang, X.Z. Zhang, Y.G. Liao, D.M. Jiang, J.Y. Zhang, Z.X. Sheng, C. Xie, Z. Peng, X.H. Zhuang, V. Bunpetch, Y.W. Zou, W.W. Huang, Q. Zhang, E.V. Alakpa, S.F. Zhang, H.W. Ouyang, Rapid printing of bio-inspired 3D tissue constructs for skin regeneration, Biomaterials 258 (2020) 120287.
[51] A.C. Stromdahl, L. Ignatowicz, G. Petruk, M. Butrym, S. Wasserstrom, A. Schmidtchen, M. Puthia, Peptide-coated polyurethane material reduces wound infection and inflammation, Acta Biomater. 128 (2021) 314–331.
[52] K. Wang, R.N. Dong, J.Z. Tang, H.C. Li, J.L. Dang, Z.X. Zhang, Z. Yu, B.L. Guo, C.G. Yi, Exosomes laden self-healing injectable hydrogel enhances diabetic wound healing via regulating macrophage polarization to accelerate angiogenesis, Chem. Eng. J. 430 (2022) 132664.
[53] H. Yang, L. Song, B.X. Sun, D. Chu, L.L. Yang, M. Li, H. Li, Y. Dai, Z. Yu, J.F. Guo, Modulation of macrophages by a paeoniflorin-loaded hyaluronic acid-based hydrogel promotes diabetic wound healing, Mater. Today Bio 12 (2021) 100139.